

Anomalous phonon magnetic moments

Swati Chaudhary,^{1,*} Carl P. Romao,^{2,3,†} and Dominik M. Juraschek⁴

¹The Institute for Solid State Physics, The University of Tokyo, Kashiwa, Chiba 277-8581, Japan

²Department of Materials, ETH Zürich, Wolfgang-Pauli-Str. 27, 8093 Zürich, Switzerland

³Department of Materials, Faculty of Nuclear Sciences and Physical Engineering,

Czech Technical University in Prague, Trojanova 13, Prague 120 00, Czech Republic

⁴Department of Applied Physics and Science Education,
Eindhoven University of Technology, 5612 AP Eindhoven, Netherlands

Circularly polarized phonons conventionally carry an angular momentum and a magnetic moment arising from circular motions of the atoms. Here, we present three anomalous cases that lead to phonon magnetic moments, which cannot be described in the conventional framework: *rotationless axial phonons*, which exhibit magnetic responses despite only carrying pseudo angular momentum, *divergent gyromagnetic ratios of phonons*, in which a magnetic moment is produced despite vanishing angular momentum, and *anisotropic gyromagnetic ratios of phonons*, which make the phonon angular momentum and magnetic moment noncollinear. Our results shed light on the origin and nature of phonon magnetism and suggest the existence of phononmagnetic hidden order.

I. INTRODUCTION

Circularly polarized phonons carry angular momentum that can be exchanged with other particles, such as photons or electrons, on fundamental timescales [1–3]. These lattice vibrations, appearing in the form of axial and chiral phonons [4–7], produce magnetic moments and hence represent a fundamental degree of freedom in crystalline solids in addition to electronic angular momentum [8–11]. The phonon magnetic moment, \mathbf{m}^{ph} , and angular momentum, \mathbf{l}^{ph} , have so-far been considered to be collinear and proportional to each other by a phonon gyromagnetic ratio, $\mathbf{m}^{ph} = \gamma^{ph}\mathbf{l}^{ph}$ [8].

The origin of angular momentum of a (quasi)particle is not always directly linked to circular motion, as is commonly exemplified by the electron spin. An alternative definition of the angular momentum can be formulated from the transformation of a wavefunction under rotation [12, 13]. For example, the variation of the phase of the electromagnetic field of light with an azimuthal angle gives rise to a twisted wavefront and therefore orbital angular momentum even for linear polarization [14]. The same principle also applies to elastic deformations and lattice vibrations with azimuthal phase variation [15–17], as well as to twisted magnon beams [18]. On the atomic length scale, phonon angular momentum can be obtained by acting the n -fold rotation operator on the phonon displacement vector [12, 19]. This form is known as phonon pseudo angular momentum (PAM) and stems from a phase difference between the motion of different atoms belonging to the same unit cell (spin PAM) or different unit cells (orbital PAM) [12]. The prototypical example of phonons carrying PAM is found in the K/K' valleys of hexagonal lattices [1, 12, 20–23]. There,

the angular momentum from circular motion and that from relative phase correlations between different atoms are intertwined. The literature to date has not considered the case of phonon eigenmodes where angular momentum arises purely from phase correlations at atomic length scales without any circular motion of atoms.

In this work, we demonstrate three cases that defy the conventional picture of the phonon magnetic moment: firstly, *rotationless axial phonons*, which possess only pseudo, but no real angular momentum, and which can generate effective phonon magnetic moments; secondly, phonons with divergent gyromagnetic ratios, in which a finite magnetic moment is generated despite vanishing angular momentum; and thirdly, anisotropic gyromagnetic ratios that cause the phonon angular momentum and magnetic moment to be noncollinear. A schematic overview is shown in Fig. 1. Because our analysis will involve both chiral and achiral phonons carrying angular momentum, we will in the following use the neutral term “axial phonons” to indicate they can be represented by the axial vector \mathbf{l} [7].

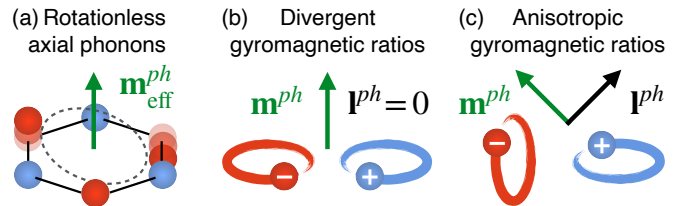


FIG. 1. Anomalous phonon magnetic moments. (a) Rotationless axial phonons can carry effective magnetic moments while containing only linear atomic motion. (b) Divergent gyromagnetic ratios produce finite magnetic moments despite vanishing angular momentum. (c) Anisotropic gyromagnetic ratios produce noncollinear phonon angular momentum and magnetic moments.

* These authors contributed equally to this work.; swatichaudhary@issp.u-tokyo.ac.jp

† These authors contributed equally to this work.; carl.romao@cvut.cz

II. PHONON ANGULAR MOMENTUM AND MAGNETIC MOMENTS

We begin by reviewing the formalism of phonon angular momentum. Real phonon angular momentum arises from circular motion of atoms around their equilibrium positions in a crystal and, for a specific phonon mode ν at a wavevector \mathbf{q} , can be written as [24]

$$\mathbf{l}_{\nu\mathbf{q}}^{ph} = \hbar \sum_{\alpha} \mathbf{l}_{\nu\mathbf{q}\alpha}^{ph} = \sum_{\alpha} \mathbf{u}_{\nu\mathbf{q}\alpha} \times \dot{\mathbf{u}}_{\nu\mathbf{q}\alpha}, \quad (1)$$

where $\mathbf{u}_{\nu\mathbf{q}\alpha}$ is the phonon displacement vector for atom α . In ionic crystals, these phonons further carry a magnetic moment produced by a circular charge current of the ions that can be written as [4, 8, 25, 26]

$$\mathbf{m}_{\nu\mathbf{q}}^{ph} = \sum_{\alpha} \mathbf{m}_{\nu\mathbf{q}\alpha}^{ph} = \hbar \sum_{\alpha} \frac{Z_{\alpha}^*}{2M_{\alpha}} \mathbf{l}_{\nu\mathbf{q}\alpha}^{ph}, \quad (2)$$

where Z_{α}^* is the Born effective charge tensor, M_{α} the atomic mass, and $Z_{\alpha}^*/(2M_{\alpha})$ the gyromagnetic ratio of atom α . This magnetic moment arises from circular charge currents and produces a Maxwellian magnetic field from the dynamical multiferroic effect [27, 28]. Its magnitude is typically on the order of the nuclear magneton, μ_n [4, 6, 8, 10, 29], but can be enhanced by up to four orders of magnitude through Maxwellian or non-Maxwellian contributions from electron- and spin-phonon coupling [9, 11, 30–36].

Phonons can further carry pseudo angular momentum (PAM) arising from phase differences between atomic motions under n -fold rotational operations [12],

$$C_n(z)\mathbf{u}_{\nu\mathbf{q}} e^{i\mathbf{R}_{\alpha l} \cdot \mathbf{q}} = e^{-i\frac{2\pi}{n}\hat{z} \cdot \mathbf{l}_{\nu\mathbf{q}}^p} \mathbf{u}_{\nu\mathbf{q}} e^{i\mathbf{R}_{\alpha l} \cdot \mathbf{q}}, \quad (3)$$

where $\mathbf{l}_{\nu\mathbf{q}}^p$ is the PAM along the rotation axis \hat{z} passing through a n -fold symmetric point in the unit cell and can take values of $\mathbf{l}_{\nu\mathbf{q}}^p = 0, \dots, (n-1)$, and $\mathbf{R}_{\alpha l}$ is the position vector for atom α in unit cell l . The phase factor can arise from a rotation of the displacement vector $\mathbf{u}_{\nu\mathbf{q}}$ directly (intracell, spin PAM), or from a rotation of the nonlocal part, $e^{i\mathbf{R}_j \cdot \mathbf{q}}$, (intercell, orbital PAM), for which $\mathbf{l}_{\nu\mathbf{q}}^p = \mathbf{l}_{\nu\mathbf{q}}^{p,s} + \mathbf{l}_{\nu\mathbf{q}}^{p,o}$. This quantized PAM arises at points in the Brillouin zone that respect n -fold rotational symmetry.

Real phonon angular momentum has been associated with the generation of magnetic fields [3, 25, 27, 37–41], whereas PAM is important for selection rules in light- and electron-phonon scattering [1, 4, 5, 12, 42, 43]. In these and other studies, the investigated phonons involve circular motions of atoms and exhibit collinear phonon angular momentum and magnetic moments. PAM in turn arises from the action of the rotational operator C_n and makes no assumptions about the circularity of the atomic motion. Hence, also purely linear motions of the atoms along the rotation axis should lead to PAM as long as there is a phase difference between them.

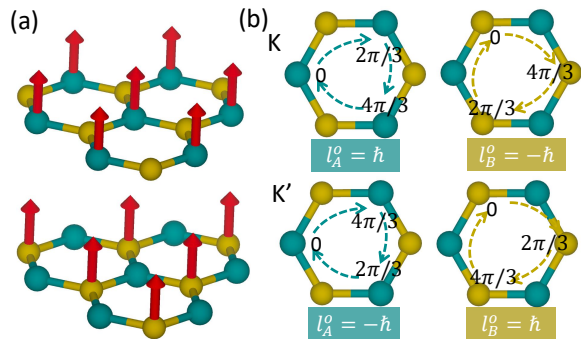


FIG. 2. Out-of-plane atomic displacements in monolayer h-BN. (a) Atomic displacement associated with the transverse acoustic modes, which correspond to the out-of-plane motion from phonons at K/K' valleys with frequencies of 9.2 THz (top) and 17.9 THz (bottom). While all eigenvectors point out of the plane, their relative motion is phase delayed as shown in (b), resembling the motion of an Euler disk. (b) K and K' valley phonons have an opposite phase difference, resulting in an orbital PAM of ± 1 . Boron atoms are shown in green and nitrogen atoms are shown in yellow.

III. ROTATIONLESS AXIAL PHONONS

We next introduce rotationless axial phonons in hexagonal materials for the simple examples of honeycomb and kagome lattices. We then derive the magnetic response for hexagonal cerium trichloride (CeCl_3), and show that they produce effective magnetic moments purely from PAM, despite vanishing $\mathbf{l}_{\nu\mathbf{q}}^{ph}$ and $\mathbf{m}_{\nu\mathbf{q}}^{ph}$. As we will be considering phonon modes of specific branches and wavevectors, we will drop the indices ν and \mathbf{q} .

A. Rotationless axial phonons in honeycomb lattices

The three-fold rotation around the center of the hexagon leads to orbital PAM that is opposite in sign for different sublattices, A and B , $l^{p,o}(A) = -l^{p,o}(B) = \pm 1$ for all phonon branches at $\mathbf{q} = K/K'$. Additionally, K/K' -valley phonons with in-plane circular motion also carry a spin PAM of $l^{p,s} = \pm 1$, resulting in a total PAM of $l^p = l^{p,s}(A) + l^{p,o}(A) = l^{p,s}(B) + l^{p,o}(B)$. The three-fold rotation symmetry enforces a total PAM of $l^p = \pm 1, 0$ modulo 3, which constrains the in-plane valley phonons to have only one sublattice moving or to exhibit opposite circular motion for the A and B sublattices. On the other hand, phonon modes with linear out-of-plane motion cannot carry any spin PAM, implying a total PAM of $l^p = l^{p,o} = \pm 1$. Given that $l^{p,o}(A) = -l^{p,o}(B) = \pm 1$, any nondegenerate valley phonon with linear out-of-plane motion must have only one sublattice moving and the total PAM about the three-fold axis passing through the center of the hexagon or through the stationary sublattice would be ± 1 . This requires broken inversion symmetry and is realized in hexagonal boron ni-

tride (h-BN). We investigate out-of-plane nondegenerate transverse acoustic K/K' phonons in monolayer h-BN in Fig. 2 (a), calculated for h-BN from first principles [44–47]. (For computational details, see Appendix A.) These phonon modes involve only the motion of one sublattice and pick up a phase of $\pm 2\pi/3$ after three-fold rotation around the center of honeycomb, as shown in Fig. 2 (b), resulting in an orbital PAM of ± 1 arising from the intercell phase difference.

B. Rotationless axial phonons in kagome lattices

In kagome lattices, each site contains three atoms related by three-fold rotation about an axis passing through the center of hexagon or through the center of the triangle in the kagome structure. This implies equal orbital PAM for all sublattices and allows spin PAM arising from the intracell phase difference for phonon modes with out-of-plane linear motion. Such phonon modes can carry both spin PAM and orbital PAM, as illustrated in Fig. 3. For K/K' -valley phonons, a three-fold rotation around the center of the hexagon results in an overall phase of $2\pi/3$ due to the phase difference between different unit cells as shown by different colors in Fig. 3(b).

Similarly, for the Γ -point phonon, the three-fold rotation around the center of hexagon or triangle in the kagome unit results in the same phase of $2\pi/3$ when different sublattices are moving out-of-plane with a phase difference of $2\pi/3$, as shown in Fig. 3(a). From group theoretical analysis, we expect that such a scenario arises for the E_u modes in the kagome magnet $\text{Co}_3\text{Sn}_2\text{S}_2$ that involves the motion of Co ions along the z axis of the crystal (see Appendix B for details). Previous studies have already suggested that E_g and E_u modes carrying real angular momentum in this material split in an applied magnetic field and hence possess a magnetic moment [48, 49]. Another example are the E_{2u} modes in FeGe that should exhibit similar properties. These phonons can become axial when time-reversal symmetry is broken either due to an applied magnetic field or magnetic ordering.

C. Magnetic response of rotationless axial phonons in cerium trichloride

For rotationless zone-center phonons, spin PAM can arise from an intracell phase difference, as we have shown for kagome lattices above. We now show that these phonons can carry effective magnetic moments and respond to applied magnetic fields, despite carrying no real magnetic moments according to Eq. (2). We use the example of the rare-earth $4f$ -paramagnet CeCl_3 , for which giant phono-magnetic and magneto-phononic effects have been discovered due to its strong orbit-lattice coupling [11, 38, 40, 50, 51]. The material crystallizes in the hexagonal space group $P6_3/m$ and exhibits one E_{1g} and one E_{2u} symmetric phonon mode at the cen-

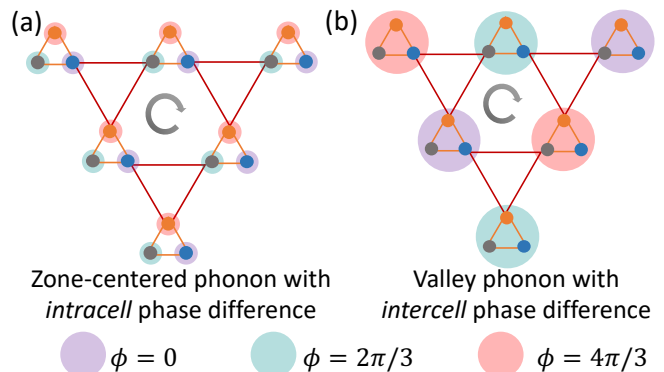


FIG. 3. Spin and orbital PAM in a kagome lattice. Phonons with out-of-plane motion in a kagome lattice can carry PAM due to intracell and intercell phase differences. A three-fold rotation of the phonon mode around a C_3 symmetric point in the lattice results in a phase of $\pm 2\pi/3$. (a) Zone-center phonon, producing a $2\pi/3$ phase difference between the three atoms on a given lattice site, leading to a spin PAM of 1 with the same sign for all sublattices under a three-fold rotation. (b) Valley phonons, with a $2\pi/3$ phase difference between the three lattice sites from neighboring unit cells, resulting in an orbital PAM under a three-fold rotation.

ter of the Brillouin zone that induce purely out-of-plane atomic motions, as illustrated in Fig. 4. (For details on CeCl_3 , see Appendix D.)

The phonon displacement vector of the E_{2u} mode at 20.5 meV can be obtained from group theory [52],

$$\mathbf{u}_{E_{2u}}^a = \frac{Q_a}{2\sqrt{6}} (0, 0, 2\hat{z}, -\hat{z}, -\hat{z}, 2\hat{z}, -\hat{z}, -\hat{z}), \quad (4)$$

$$\mathbf{u}_{E_{2u}}^b = \frac{Q_b}{2\sqrt{2}} (0, 0, 0, \hat{z}, -\hat{z}, 0, \hat{z}, -\hat{z}), \quad (5)$$

with basis $(\text{Ce}_A^{3+}, \text{Ce}_B^{3+}, \text{Cl}_{1A}^-, \text{Cl}_{2A}^-, \text{Cl}_{3A}^-, \text{Cl}_{1B}^-, \text{Cl}_{2B}^-, \text{Cl}_{3B}^-)$, and where $Q_{a/b}$ are the normal mode coordinates (amplitudes) of the two orthogonal components a and b in units of $\text{\AA}\sqrt{\text{amu}}$, where amu is the atomic mass unit. The circular superposition of two components of the E_{2u} mode, $\mathbf{Q}^\pm = \mathbf{u}_{E_{2u}}^a \pm i\mathbf{u}_{E_{2u}}^b$, results in axial phonon given by

$$\mathbf{Q}^\pm = \frac{Q}{\sqrt{6}} \hat{z} \left(0, 0, 1, e^{\pm i\frac{2\pi}{3}}, e^{\pm i\frac{4\pi}{3}}, 1, e^{\pm i\frac{2\pi}{3}}, e^{\pm i\frac{4\pi}{3}} \right), \quad (6)$$

which indicates that the three Cl^- ions in a given xy plane around the Ce^{3+} ions are moving in z direction but with a relative phase difference of $\pm 2\pi/3$ as shown in Fig. 4(b). This leads to spin PAM of $l^{p,s} = \pm 1$ as evident by the three-fold rotation on the phonon mode:

$$C_3(z)\mathbf{Q}^\pm = e^{-i\frac{2\pi}{3}l^{p,s}}\mathbf{Q}^\pm. \quad (7)$$

It is known that in the presence of a magnetic field, phonons with real angular momentum can exhibit the Zeeman effect, which in turn can be used to define an effective phonon magnetic moment. We now calculate the splitting of these axial phonons in the presence of an

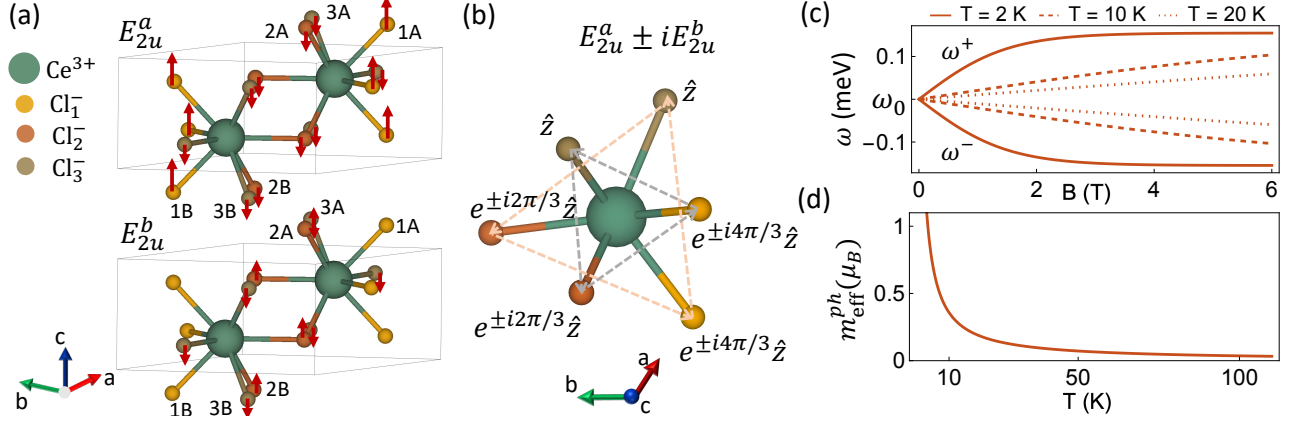


FIG. 4. Axial E_{2u} mode and its magnetic response. (a) Displacement associated with the two orthogonal components of the E_{2u} mode. (b) A circular superposition of the two components results in a relative phase difference between displacements of different atoms within the same unit cell, leading to a phonon spin pseudo angular momentum. (c) Phonon Zeeman splitting, $\Delta\omega_{ph}$ of the axial E_{2u} mode in the presence of an external magnetic field. (d) Temperature dependence of the effective phonon magnetic moment, m_{eff}^{ph} .

applied magnetic field along the direction of three-fold rotation axis. We use the formalism developed in Ref. [11] to compute the phonon frequency splitting arising from orbit-lattice coupling which depends on the polarization state of phonon eigenmodes. In this mechanism, phonons hybridize with orbital excitations on the magnetic ion that carry finite angular momentum, resulting in a frequency splitting that depends on the phonon angular momentum, see Appendixes C and D for details. Here, we find the phonon eigenmodes, \mathbf{Q}^{\pm} which carry opposite PAM, exhibit a frequency splitting that depends on the magnetic field and temperature, as shown in Fig. 4(c). It is linear for small B and saturates to a value of 0.3 meV for increasing magnetic fields. In contrast to Eq. (2), we can use this PAM-dependent phonon frequency splitting to define an effective gyromagnetic ratio and phonon magnetic moment as

$$m_{\text{eff}}^{ph} = \gamma_{\text{eff}}^{ph} l^{ph} = \frac{1}{2} \left. \frac{\partial \Delta\omega_{ph}}{\partial B} \right|_{B=0}, \quad (8)$$

where $\Delta\omega_{ph}$ denotes the energy splitting (in meV) of axial phonons with opposite PAM due to the applied magnetic field. Using Eq. (8), we find an effective phonon magnetic moment of the order of 1 μ_B at a temperature of $T = 2$ K, which decreases monotonically with temperature as shown in Fig. 4(d). While the effective phonon magnetic moment characterizes the phononic response to an applied magnetic field, it also produces a real magnetic moment arising from spin polarization in the paramagnetic material that is given by $m_{\text{real}}^{ph} = \chi_m m_{\text{eff}}^{ph}$, where χ_m is the magnetic susceptibility. Because $\chi_m \sim 10^{-4}$ [38], the real magnetic moment is on the order of the nuclear magneton. The phonon Zeeman effect has not yet been measured for infrared-active or silent modes in CeCl₃, however the rotationless Raman-active E_{1g} mode was shown to exhibit a strong Zeeman splitting in early

experiments [51]. Our results demonstrate that circular atomic motion and therefore real phonon angular momentum is neither a necessary requirement for electron spin to phonon angular momentum coupling, nor for magnetic responses of axial phonons.

Now that we have shown that effective phonon magnetic moments can arise solely from PAM, we will consider two more anomalous behaviors of phonon modes, in which the magnetic moment is not directly proportional to the real angular momentum.

IV. DIVERGENT GYROMAGNETIC RATIOS OF PHONONS

Axial phonons exhibit both circular and, as we have shown, linear motions of the atoms [29]. If ionic sublattices revolve in opposite directions, phonons without net angular momentum can still produce phonon magnetism. For example, in a crystal with one cation (+) and one anion (-) per unit cell, the effective charges are equal in magnitude and opposite in sign, $Z_+^* = -Z_-^*$. For a phonon mode with $\mathbf{l}_+^{ph} = -\mathbf{l}_-^{ph}$, the phonon angular momentum in Eq. (1) vanishes, whereas the phonon magnetic moment in Eq. (2) remains nonzero. Accordingly, the phonon gyromagnetic ratio, defined as $\gamma^{ph} = \frac{|\mathbf{m}^{ph}|}{|l^{ph}|}$, diverges. This ideal case is approximated in monolayer h-BN. Axial phonons have previously been studied in h-BN [53] and in heterostructures containing h-BN [54, 55], where they show a phonon band structure similar to the noncentrosymmetric transition metal dichalcogenides [12]. Here, we demonstrate the existence of near-divergent gyromagnetic ratios in Fig. 5 using the calculated phononic properties of h-BN [44–47].

As shown in Fig. 5a, the longitudinal acoustic (LA) phonon branch is fully circularly polarized at $\mathbf{q} = K$,

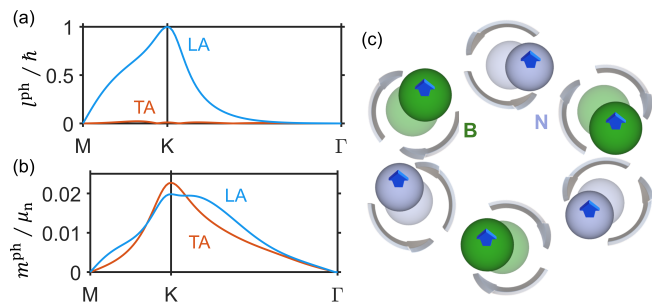


FIG. 5. (a) Phonon angular momentum, l^{ph} , and (b) phonon magnetic moment, m^{ph} , (in units of the nuclear magneton, μ_n) of the longitudinal acoustic (LA) and fast transverse acoustic (TA) bands of monolayer h-BN, shown as a function of wavevector along the $M (\frac{1}{2} 0 0) - K (\frac{1}{3} \frac{1}{3} 0) - \Gamma (0 0 0)$ trajectory in reciprocal space. (c) Atomic displacements in the TA band at the K point, where B and N atoms revolve in opposite directions around their equilibrium positions (transparent spheres). This leads to a near-vanishing net angular momentum, counter-aligned for the two sublattices, but a substantial net magnetic moment (blue arrows), co-aligned for the two sublattices due to their opposite effective charges.

corresponding to circular motions of the B sublattice, while the fast transverse acoustic (TA) branch has nearly vanishing phonon angular momentum. However, the TA branch still possesses a substantial phonon magnetic moment (Fig. 5b) due to the clockwise motions of the B cations combined with the counterclockwise motions of the N anions (Fig. 5c), leading to a near divergence of the gyromagnetic ratio.

V. ANISOTROPIC GYROMAGNETIC RATIOS OF PHONONS

Divergent gyromagnetic ratios of phonons can be expanded to the more general phenomenon of anisotropic gyromagnetic ratios of phonons. This phenomenon occurs when the atomic phonon angular momentum vectors, \mathbf{l}_α^{ph} , of the different ionic sublattices are not aligned. We show here that this misalignment occurs at arbitrary \mathbf{q} even in a highly symmetric crystal with only two independent atomic positions. The misalignment leads to a noncollinear local arrangement of the magnetic moments arising from circular atomic motions, \mathbf{m}_α^{ph} , and a difference in spatial orientation between the phonon angular momentum and phonon magnetic moment vectors. Accordingly, both quantities are connected by a tensorial phonon gyromagnetic ratio, $\mathbf{m}^{ph} = \underline{\underline{\gamma}}^{ph} \mathbf{l}^{ph}$, where $\mathbf{m}^{ph} \nparallel \mathbf{l}^{ph}$.

We demonstrate anisotropic gyromagnetic ratios of phonons for the example of noncentrosymmetric gallium arsenide (GaAs) in Fig. 6, using phonon data computed from first principles [56, 57], for details see Appendix A. The optical phonons between the L and W points involve noncoplanar circular motions of the atoms. The

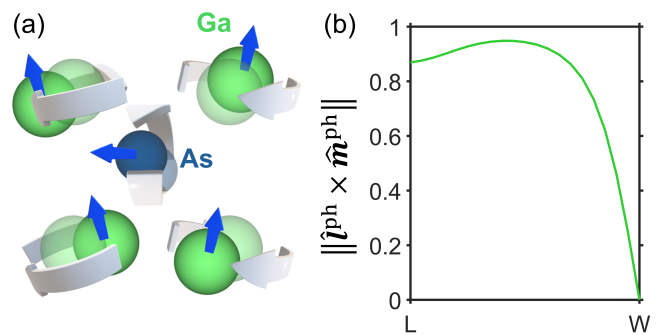


FIG. 6. (a) The noncollinear nature of the atomic moments (blue arrows) in GaAs, arising from the orbital motions of the atoms (spheres) around their average positions (transparent spheres), is shown schematically for a phonon halfway between $L (\frac{1}{2} \frac{1}{2} \frac{1}{2})$ and $W (\frac{1}{2} \frac{1}{4} \frac{3}{4})$. This noncollinearity gives rise to a difference between the spatial orientation of the phonon angular momentum, \mathbf{l}^{ph} , and magnetic moment vectors, \mathbf{m}^{ph} . (b) Magnitude of the cross product of the unit vectors, $\|\hat{\mathbf{l}}^{ph} \times \hat{\mathbf{m}}^{ph}\|$, for the highest energy optical branch along the $L - W$ trajectory, showing the effect of the anisotropic phonon gyromagnetic ratio.

magnetic moments of the Ga ions are primarily aligned along the z axis of the crystal, while those of the As ions are oriented in the xy plane (Fig. 6a). In combination with the differing gyromagnetic ratios of the two ions, a phonon magnetic moment emerges that is nearly orthogonal to the phonon angular momentum along most of the $L - W$ direction (Fig. 6b).

VI. DISCUSSION

The rotationless axial phonons presented here challenge the conventional understanding that circular atomic motion is required to induce spin PAM and phonon magnetic moments and shows that both can be achieved with only linear atomic motion. The large effective magnetic moment of the rotationless E_{2u} mode in CeCl_3 suggests that coherent excitation with ultrashort mid-infrared pulses can induce strong effective magnetic fields, akin to those from conventional circularly polarized phonons [38, 40, 58]. These phonons may also couple to intrinsic orders with atomic scale phase structures, such as chiral charge-density waves [59–61], or spin-density waves [62]. This opens possibilities of using phonons to detect and manipulate generalized time-reversal symmetry breaking orders, enabling probes of otherwise hidden orders, as proposed in recent work [63].

Phonons exhibiting anisotropic gyromagnetic ratios in the simple and highly symmetric materials studied here suggest similar phenomena occur more broadly in noncentrosymmetric crystals. We expect these phonons to produce unique effects such as a planar Zeeman effect, in which the applied magnetic field is perpendicular to the angular momentum. During the review of this

manuscript, an orthogonal Einstein-de Haas effect was predicted for anisotropic gyromagnetic ratios of electrons [64]. The anisotropic gyromagnetic ratios of phonons in our case could reciprocally produce an orthogonal phonon Barnett effect. Together with divergent gyromagnetic ratios, these phonons raise fundamental question of whether angular momentum or the phonon magnetic moment is the key quantity in spin-phonon coupling. Decoupling these quantities are anticipated to have profound implications for ultrafast magnetism, spin transport [65, 66], and phonon Hall effects [67–70].

Anisotropic and divergent gyromagnetic ratios of phonons further point toward hidden orders and multipolar degrees of freedom encoded in lattice excitations [71]. For example, the phonons in Fig. 6 clearly lead to a magnetization with moments of higher order than the dipole, allowing them to couple to magnetic-field gradients and electric fields [72]. The interactions between axial phonons and spin-polarized electrons could be affected by such higher-order multipoles, especially in cases where the magnetic ions themselves exhibit multipolar order [71, 73]. Such magnetic multipoles associated with phonons could be detected experimentally in X-ray or neutron scattering experiments [74, 75].

ACKNOWLEDGMENTS

S.C. acknowledges support from JSPS KAKENHI No. JP23H04865, MEXT, Japan. C.P.R. acknowledges support from the project FerrMion of the Ministry of Education, Youth and Sports, Czech Republic, co-funded by the European Union (CZ.02.01.01/00/22_008/0004591), the European Union and Horizon 2020 through grant no. 810451, and ETH Zurich. D.M.J. acknowledges support from the ERC Starting Grant CHIRALPHONONICS, no. 101166037. Computational resources were provided by the Swiss National Supercomputing Center (CSCS) under project ID s1128.

Appendix A: Computational details

The phonon energies and eigenvectors of monolayer h-BN were obtained using density functional perturbation theory with the Abinit software package (v. 10) [44]. Norm-conserving pseudopotentials were used as received from the Abinit library. The PBE GGA exchange–correlation functional [45] was used with the vdW-DFT-D3(BJ) dispersion correction of Grimme [46]. A plane-wave basis set energy cutoff of 30 Ha and a $16 \times 16 \times 1$ grid of \mathbf{k} -points were chosen following convergence studies. The structure was relaxed to an internal pressure of -7 MPa, and an $8 \times 8 \times 1$ grid of \mathbf{q} -points was then used for the phonon calculations. Computational data are publicly available from Ref. [47]. DFT-calculated phonon energies and eigenvectors of GaAs were obtained from the Materials Project database [56, 57]. The phonon

angular momentum was obtained from the phonon eigenvectors following Eq. (1); the phonon magnetic moments were obtained following Eq. (2).

Appendix B: Group theoretical analysis of phonon modes in $\text{Co}_3\text{Sn}_2\text{S}_2$

In this section, we present group theory based arguments for the existence of phonons modes with out-of-plane motion and finite PAM in Kagome Weyl semimetal $\text{Co}_3\text{Sn}_2\text{S}_2$. This material crystallizes in the trigonal (rhombohedral) space group $R\bar{3}m$ (No. 166), adopting a shandite-type structure. The Wyckoff positions in the hexagonal setting are Sn1 (site 3a), Sn2 (3b), S (6c), and Co (9d). Most interestingly, Co atoms which reside on the 9d Wyckoff position are arranged on two-dimensional kagome lattices stacked along the crystal c axis. This structure gives rise to a total of 21 phonon modes with three acoustic and 18 optical modes which decompose into $A_{1g} \oplus E_g \oplus A_{1u} \oplus 5A_{2u} \oplus 6E_u$ irreducible representations.

We calculate the basis functions for E_u modes using SAM on Bilbao crystallographic server [76] and found that three E_u mode basis functions involve the motion of Co ion as depicted in table I. The chiral superposition of $E_u(a)$ and $E_u(b)$ modes result in in-plane circular motion for the first two basis vectors shown in the table. On the other hand, the third basis vector E_u^3 involves only out-of-plane motion. The chiral superposition of $E_u^3(a)$ and $E_u^3(b)$ modes would result in a relative phase difference on Co atoms Co_1 , Co_2 , Co_3 located at three positions $(\frac{1}{2}, 0, \frac{1}{2})$, $(0, \frac{1}{2}, \frac{1}{2})$, and $(\frac{1}{2}, \frac{1}{2}, \frac{1}{2})$, respectively which are related by three-fold rotation about z-axis passing through $(0, 0, 0)$. It can be seen explicitly by writing the basis vectors E_u^3 in the basis of $(\text{Co}_1, \text{Co}_2, \text{Co}_3)$:

$$Q^\pm = E_u^3(a) \pm iE_u^3(b) = -\sqrt{\frac{2}{3}} \begin{pmatrix} e^{-i2\pi/3} \hat{z}, \hat{z}, e^{i2\pi/3} \hat{z} \end{pmatrix} \quad (\text{B1})$$

and under three-fold rotation $C_3(z)$ ($\text{Co}_1, \text{Co}_2, \text{Co}_3$)= $(\text{Co}_2, \text{Co}_3, \text{Co}_1)$ which results in:

$$\begin{aligned} C_3(z) (Q^\pm) &= -e^{\pm i2\pi/3} \sqrt{\frac{2}{3}} \begin{pmatrix} e^{-i2\pi/3} \hat{z}, \hat{z}, e^{i2\pi/3} \hat{z} \end{pmatrix} \\ &= e^{\pm i2\pi/3} Q^{pm}. \end{aligned} \quad (\text{B2})$$

This shows how the out-of-plane basis vectors of E_u modes in $\text{Co}_3\text{Sn}_2\text{S}_2$ can carry PAM.

Appendix C: General derivation of effective phonon magnetic moments from orbit-lattice coupling

In this section, we follow Ref. [11] to calculate the splitting of axial phonons. We begin by considering a degenerate phonon mode with two components that is described

Co atom	Position	$E_u^1(a)$	$E_u^1(b)$	$E_u^2(a)$	$E_u^2(b)$	$E_u^3(a)$	$E_u^3(b)$
\mathbf{X}_1	$(\frac{1}{2}, 0, \frac{1}{2})$	$\frac{1}{\sqrt{3}}$	\cdot	$\frac{1}{\sqrt{12}}$	$\frac{\sqrt{3}}{\sqrt{12}}$	\cdot	\cdot
\mathbf{Y}_1		\cdot	$\frac{1}{\sqrt{3}}$	$-\frac{1}{\sqrt{12}}$	$\frac{1}{\sqrt{12}}$	\cdot	\cdot
\mathbf{Z}_1		\cdot	\cdot	\cdot	\cdot	$\frac{1}{\sqrt{6}}$	$\frac{1}{\sqrt{2}}$
\mathbf{X}_2	$(0, \frac{1}{2}, \frac{1}{2})$	$\frac{1}{\sqrt{3}}$	\cdot	$\frac{-2}{\sqrt{12}}$	\cdot	\cdot	\cdot
\mathbf{Y}_2		\cdot	$\frac{1}{\sqrt{3}}$	\cdot	$\frac{-2}{\sqrt{12}}$	\cdot	\cdot
\mathbf{Z}_2		\cdot	\cdot	\cdot	\cdot	$\frac{-2}{\sqrt{6}}$	\cdot
\mathbf{X}_3	$(\frac{1}{2}, \frac{1}{2}, \frac{1}{2})$	$\frac{1}{\sqrt{3}}$	\cdot	$\frac{1}{\sqrt{12}}$	$-\frac{\sqrt{3}}{\sqrt{12}}$	\cdot	\cdot
\mathbf{Y}_3		\cdot	$\frac{1}{\sqrt{3}}$	$\frac{\sqrt{3}}{\sqrt{12}}$	$\frac{1}{\sqrt{12}}$	\cdot	\cdot
\mathbf{Z}_3		\cdot	\cdot	\cdot	\cdot	$\frac{1}{\sqrt{6}}$	$-\frac{1}{\sqrt{2}}$

TABLE I. Basis functions for the E_u irreducible representation at Wyckoff position 9d in $R\bar{3}m$.

by the Hamiltonian

$$H_{ph} = \omega_0(a^\dagger a + b^\dagger b). \quad (\text{C1})$$

We only consider phonon modes near the Brillouin-zone center and can accordingly drop the momentum dependence in the phonon operators and energies. In order to account for the effect of orbital-lattice coupling on the phonon spectrum, we use a Green's function formalism. For the non-interacting system, the Green's function matrix is given by

$$\mathbf{D}_0(\omega) = \begin{pmatrix} D_0^{aa}(\omega) & 0 \\ 0 & D_0^{bb}(\omega) \end{pmatrix}, \quad (\text{C2})$$

where the components are given by

$$D_0^{aa}(\omega) = D_0^{bb}(\omega) = \frac{2\omega_0}{\omega^2 - \omega_0^2}. \quad (\text{C3})$$

The phonon frequency, ω_0 , can be trivially retrieved by solving $\text{Det}(\mathbf{D}_0^{-1}(\omega)) = 0$.

We next consider the electronic Hamiltonian

$$H_{el} = \sum_{i=1}^4 \varepsilon_i c_i^\dagger c_i, \quad (\text{C4})$$

where c_i^\dagger and c_i are the creation and annihilation operators for electrons in state i on the magnetic ion. We focus on the case where these states are two Kramers doublets represented by states $(|1\rangle, |2\rangle)$ and $(|3\rangle, |4\rangle)$.

Next, we consider an orbit-lattice interaction of this form:

$$H_{el-ph} = V^a + V^b, \quad (\text{C5})$$

where

$$V^a = \sum_{i,j} g(a^\dagger + a)\Gamma_{ij}^a = g(a^\dagger + a)(c_3^\dagger c_1 + c_1^\dagger c_3) - g(a^\dagger + a)(c_4^\dagger c_2 + c_2^\dagger c_3), \quad (\text{C6})$$

$$V^b = \sum_{i,j} g(a^\dagger + a)\Gamma_{ij}^a = ig(b^\dagger + b)(c_3^\dagger c_1 - c_1^\dagger c_3) + ig(b^\dagger + b)(c_4^\dagger c_2 - c_4^\dagger c_3). \quad (\text{C7})$$

The new phonon Green's function after including these interactions is:

$$\mathbf{D}^{-1} = \begin{pmatrix} \frac{\omega^2 - \omega_0^2}{2\omega_0} - \tilde{g}^2 \left(\frac{f_1 \Delta_1}{\omega^2 - \Delta_1^2} + \frac{f_2 \Delta_2}{\omega^2 - \Delta_2^2} \right) & i\tilde{g}^2 \left(-\frac{f_1 \omega}{\omega^2 - \Delta_1^2} + \frac{f_2 \omega}{\omega^2 - \Delta_2^2} \right) \\ -i\tilde{g}^2 \left(-\frac{f_1 \omega}{\omega^2 - \Delta_1^2} + \frac{f_2 \omega}{\omega^2 - \Delta_2^2} \right) & \frac{\omega^2 - \omega_0^2}{2\omega_0} - \tilde{g}^2 \left(\frac{f_1 \Delta_1}{\omega^2 - \Delta_1^2} + \frac{f_2 \Delta_2}{\omega^2 - \Delta_2^2} \right) \end{pmatrix}, \quad (\text{C8})$$

where $\tilde{g}^2 = 2g^2$, $\Delta_1 = \varepsilon_{31}$, $\Delta_2 = \varepsilon_{42}$, f_i is the occupation of i^{th} electronic band and we assume the excited state to be unoccupied, $f_3 = f_4 = 0$. The modified energies can then be obtained by solving $\text{Det}(\mathbf{D}^{-1}) = 0$.

When a magnetic field $\mathbf{B} = B \hat{z}$ is applied, electronic

transition energies are modified as follows:

$$\Delta_1 = \Delta - \gamma B, \quad \Delta_2 = \Delta + \gamma B, \quad (\text{C9})$$

where $\gamma = \mu_{ex}^{el} - \mu_{gs}^{el}$ depends on the magnetic moment of the ground- and excited-state doublets. Lifting the degeneracy of the ground-state doublet leads to asymmetric populations of the ground-state energy levels, $f_{12} \neq 0$. Accordingly, the secular equation, $\text{Det}(\mathbf{D}^{-1}(\omega)) = 0$ for \mathbf{D}^{-1} given by Eq. (C8) becomes:

$$(\omega^2 - \omega_0^2)(\omega^2 - \Delta^2) - 2\tilde{g}^2 f_0 \omega_0 \Delta + 2\omega (B\gamma(\omega^2 - \omega_0^2) + \tilde{g}^2 \omega_0 f_{21}) + \gamma B (\gamma B(\omega^2 - \omega_0^2) + 2\tilde{g}^2 \omega_0 f_{21}) = 0, \quad (\text{C10})$$

$$(\omega^2 - \omega_0^2)(\omega^2 - \Delta^2) - 2\tilde{g}^2 f_0 \omega_0 \Delta - 2\omega (B\gamma(\omega^2 - \omega_0^2) + \tilde{g}^2 \omega_0 f_{21}) + \gamma B (\gamma B(\omega^2 - \omega_0^2) + 2\tilde{g}^2 \omega_0 f_{21}) = 0. \quad (\text{C11})$$

These two equations are not equivalent and there is a term linear in ω that indicates a frequency splitting of phonon and electronic excitations. Given that the orbit-lattice coupling is weak and the electronic excitations are off-resonant from phonons, we can assume that phonon energies are modified only slightly and have the form $\omega_{ph}^\pm = \Omega_{ph} (1 \mp \eta)$ which gives:

$$\begin{aligned} \Omega_{ph}\eta &= \frac{\gamma B(\Omega_+^2 - \omega_0^2) + \tilde{g}^2 \omega_0 f_{21}}{\Omega_{ph}^2 - \Omega_{el}^2 + \gamma^2 B^2} \\ &= \frac{\gamma B(\Omega_+^2 - \omega_0^2) + \tilde{g}^2 \omega_0 \tanh\left(\frac{\mu_{gs}^{el} B}{k_B T}\right)}{\sqrt{(\omega_0^2 - \Delta^2)^2 + 8\tilde{g}^2 f_0 \omega_0 \Delta + \gamma^2 B^2}}. \end{aligned} \quad (\text{C12})$$

where f_{21} was replaced by $-\tanh\left(\frac{\mu_{gs}^{el} B}{k_B T}\right)$ with μ_{gs}^{el} representing the magnetic moment of ground state manifold as the system is paramagnetic. For the off-resonant case, we can assume $|\Delta - \omega_0| \gg \gamma B$ and therefore neglect the linear B term in the numerator and the quadratic one in the denominator. The off-resonant case is a reasonable assumption, as $\gamma B \sim 0.5$ meV in strong magnetic fields of $B = 10$ T, whereas often $|\Delta - \omega_0| > 10$ meV. As a result, the splitting of the phonon frequencies can be written as

$$\frac{\omega_{ph}^+ - \omega_{ph}^-}{\omega_{ph}(B=0)} \approx \frac{2\tilde{g}^2}{\sqrt{(\omega_0^2 - \Delta^2)^2 + 8\tilde{g}^2 f_0 \omega_0 \Delta}} \tanh\left(\frac{\mu_{gs}^{el} B}{k_B T}\right), \quad (\text{C13})$$

which is the main expression used to evaluate the splitting shown in Fig. 4.

Appendix D: Symmetry properties and E_{2u} modes of CeCl_3

The rare-earth trihalide CeCl_3 , shown in Fig. 7(a), crystallizes in the space group no. 176 (point group $6/m$) and its primitive unit cell contains eight atoms. The two Ce^{3+} ions are located at the $2c$ Wyckoff positions and the six Cl^- ions are located at the $6h$ Wyckoff positions. Each Ce^{3+} ion has nine nearest neighbors arranged in three different planes. In each plane, the three Cl^- atoms are related by a three-fold rotation along a z axis passing through Ce^{3+} ion or the center of the hexagon. This structure leads to 21 optical phonon modes out of which two modes (E_{1g} and E_{2u}) have purely out-of-plane motion [52] consisting of the irreducible representations $2A_g \oplus 1A_u \oplus 2B_g \oplus 2B_u \oplus 1E_{1g} \oplus 3E_{2g} \oplus 2E_{1u} \oplus 1E_{2u}$ [40]. Using SAM on Bilbao crystallographic server [52], we found

that out of these seven doubly degenerate phonons, two modes (E_{1g} and E_{2u}) have purely out-of-plane motion.

The ground-state configuration of the Ce^{3+} ($4f^1$) ion is given by a nearly free-ion configuration of a $L = 3, S = 1/2$ state in accordance with Hund's rule. The spin-orbit coupling splits this 14 dimensional space into $J = 5/2$ and $J = 7/2$ total angular momentum sectors and the ground-state is given by the six-dimensional $J = 5/2$ ($^2F_{5/2}$) state as shown in Fig. 7 (b). Since there is only one electron in the $4f$ orbitals, the wavefunctions of different states in this multiplet can be written as

$$\begin{aligned} |J = 5/2, m_j = \pm 5/2\rangle &= -\sqrt{\frac{1}{7}} |m_l = \pm 2, m_s = \pm 1/2\rangle \\ &\quad + \sqrt{\frac{6}{7}} |m_l = \pm 3, m_s = \mp 1/2\rangle, \end{aligned} \quad (\text{D1})$$

$$\begin{aligned} |J = 5/2, m_j = \pm 3/2\rangle &= -\sqrt{\frac{2}{7}} |m_l = \pm 1, m_s = \pm 1/2\rangle \\ &\quad + \sqrt{\frac{5}{7}} |m_l = \pm 2, m_s = \mp 1/2\rangle, \end{aligned} \quad (\text{D2})$$

$$\begin{aligned} |J = 5/2, m_j = \pm 1/2\rangle &= -\sqrt{\frac{3}{7}} |m_l = \pm 0, m_s = \pm 1/2\rangle \\ &\quad + \sqrt{\frac{4}{7}} |m_l = \pm 1, m_s = \mp 1/2\rangle, \end{aligned} \quad (\text{D3})$$

where $|m_l, m_s\rangle$ is a $4f$ orbital state with orbital quantum number m_l and spin quantum number m_s . The CEF further splits the states into three Kramers doublets $|\pm 5/2\rangle$, $|\pm 1/2\rangle$, and $|\pm 3/2\rangle$ with energies 0 meV, 5.82 meV, 14.38 meV, respectively [51].

We use a point-charge model to describe the crystal electric field of the system, in which the potential energy of an electron at position \mathbf{r} from Ce^{3+} nucleus due to the n -th Cl^- ion is given by

$$V(\mathbf{R}_n, \mathbf{r}) = \frac{e^2}{4\pi\epsilon_0} \frac{1}{|\mathbf{R}_n - \mathbf{r}|}, \quad (\text{D4})$$

where $\mathbf{R}_n = \mathbf{R}_{0,n} + \mathbf{u}_n$ is the displacement of the n -th ligand ion from Ce^{3+} nucleus, which depends on the equilibrium displacement, $\mathbf{R}_{0,n}$, and the relative lattice displacement, \mathbf{u}_n , arising from the phonon.

The perturbation introduced by a given phonon mode can be obtained by a Taylor expansion of the potential in the lattice displacement \mathbf{u}_n to linear order, which is done in Mathematica using the built-in series expansion

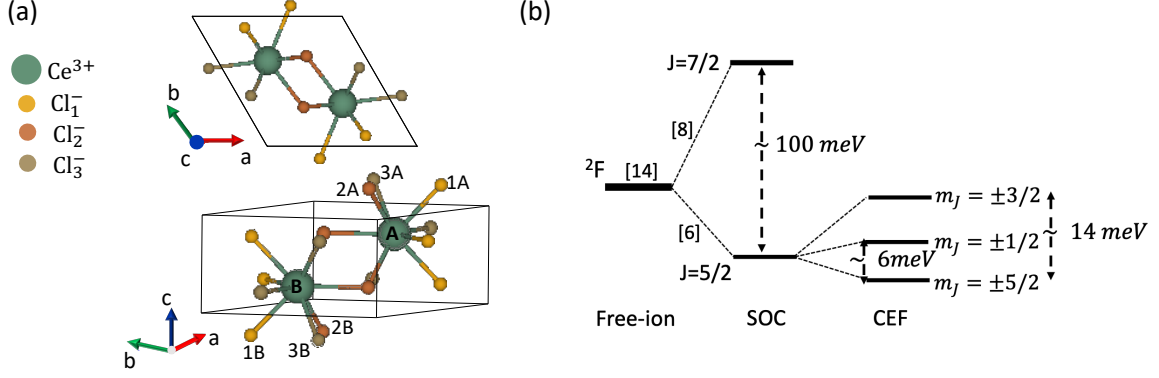


FIG. 7. (a) CeCl₃ crystal structure along two directions. (b) Electronic energy levels of the Ce³⁺ ion. The energy levels compared to the free ion are split by spin-orbit coupling and by the crystal electric field, resulting in three Kramer's doublets, of which $\pm 5/2$ is the ground state.

function which evaluates

$$\partial_{u_n^\alpha} \partial_{r^\beta} \partial_{r^\gamma} \left(\frac{1}{|\mathbf{R}_n - \mathbf{r}|} \right) \Big|_{\mathbf{R}_n = \mathbf{R}_{0,n}, r=0}. \quad (\text{D5})$$

The E_{2u} phonon lowers the symmetry around the magnetic ion and for the lattice distortion induced by this phonon, the first order term for the change in Coulomb potential is given by:

$$V(E_{1g}(a)) = [-0.1xz + 0.066yz] Q_a \frac{\text{eV}}{\text{\AA}^3 \sqrt{\text{amu}}}, \quad (\text{D6})$$

$$V(E_{1g}(b)) = [0.066xz + 0.1yz] Q_b \frac{\text{eV}}{\text{\AA}^3 \sqrt{\text{amu}}}. \quad (\text{D7})$$

Now, we can express $xz = r^2 \sin \theta \cos \theta \cos \phi$ and $yz = r^2 \sin \theta \cos \theta \sin \phi$ in spherical coordinates. The electronic states on Ce³⁺ ion can be written in terms of $|L=3, m=m_l\rangle$ which have wavefunction $\langle r|L=3, m=m_l\rangle = R(r)Y_3^{m_l}(\theta, \phi)$. This allows us to calculate the matrix elements between different 4f states and the only nonzero terms are given by

$$\langle m = \pm 3 | xz | m = \pm 2 \rangle = \mp \langle r^2 \rangle \frac{1}{3\sqrt{6}}, \quad (\text{D8})$$

$$\langle m = \pm 2 | xz | m = \pm 1 \rangle = \mp \langle r^2 \rangle \frac{1}{3\sqrt{10}}, \quad (\text{D9})$$

$$\langle m = \pm 1 | xz | m = \pm 0 \rangle = \mp \langle r^2 \rangle \frac{1}{3\sqrt{75}}, \quad (\text{D10})$$

$$\langle m = \pm 3 | yz | m = \pm 2 \rangle = \langle r^2 \rangle \frac{i}{3\sqrt{6}}, \quad (\text{D11})$$

$$\langle m = \pm 2 | yz | m = \pm 1 \rangle = \langle r^2 \rangle \frac{i}{3\sqrt{10}}, \quad (\text{D12})$$

$$\langle m = \pm 1 | yz | m = 0 \rangle = \langle r^2 \rangle \frac{i}{3\sqrt{75}}. \quad (\text{D13})$$

Using these values for states given in Eq. (D1)-(D3), we obtain the matrices for xz and yz operators

$$H_1(xz) = -\frac{2}{7\sqrt{5}} \langle r^2 \rangle \begin{pmatrix} \left| \frac{5}{2}, \pm \frac{5}{2} \right\rangle & \left| \frac{5}{2}, \pm \frac{3}{2} \right\rangle \\ \left| \frac{5}{2}, \pm \frac{5}{2} \right\rangle & 0 & \pm 1 \\ \left| \frac{5}{2}, \pm \frac{3}{2} \right\rangle & \pm 1 & 0 \end{pmatrix}, \quad (\text{D14})$$

$$H_1(yz) = \frac{2}{7\sqrt{5}} \langle r^2 \rangle \begin{pmatrix} \left| \frac{5}{2}, \pm \frac{5}{2} \right\rangle & \left| \frac{5}{2}, \pm \frac{3}{2} \right\rangle \\ \left| \frac{5}{2}, \pm \frac{5}{2} \right\rangle & 0 & i \\ \left| \frac{5}{2}, \pm \frac{3}{2} \right\rangle & -i & 0 \end{pmatrix} \quad (\text{D15})$$

where $\langle r^2 \rangle = \int_0^\infty r^2 |R(r)|^2 r^2 dr$ is the mean-square 4f-electron radius. We can write the phonon displacements as

$$Q_a = \frac{\hbar}{\sqrt{\hbar\omega_0}} (a + a^\dagger) = \frac{0.06 \text{\AA} \sqrt{\text{eV amu}}}{\sqrt{\hbar\omega_0}} (a + a^\dagger), \quad (\text{D16})$$

$$Q_b = \frac{\hbar}{\sqrt{\hbar\omega_0}} (b + b^\dagger) = \frac{0.06 \text{\AA} \sqrt{\text{eV amu}}}{\sqrt{\hbar\omega_0}} (b + b^\dagger), \quad (\text{D17})$$

where we restored \hbar and $\hbar\omega_0$ is the energy of phonon mode. As a result, the orbit-lattice coupling operators now takes the following form

$$H_{el-ph} = (a^\dagger + a)\hat{O}_a + (b^\dagger + b)\hat{O}_b, \quad (\text{D18})$$

where

$$\hat{O}_a = ge^{i\theta} \left| + \frac{5}{2} \right\rangle \left\langle + \frac{3}{2} \right| - ge^{-i\theta} \left| - \frac{5}{2} \right\rangle \left\langle - \frac{3}{2} \right| + \text{h.c.}, \quad (\text{D19})$$

$$\hat{O}_b = ige^{i\theta} \left| + \frac{5}{2} \right\rangle \left\langle + \frac{3}{2} \right| + ige^{-i\theta} \left| - \frac{5}{2} \right\rangle \left\langle - \frac{3}{2} \right| + \text{h.c.} \quad (\text{D20})$$

Here, we combined Eqs. (D7), (D15), and (D17) in order to obtain $g = -\sqrt{0.1^2 + 0.066^2} \frac{2}{7\sqrt{5}} \langle r^2 \rangle \frac{0.06}{\sqrt{\omega_0}} \text{eV}^{3/2} / \text{\AA}^2$ and $\tan(\theta) = 0.66/0.1$. This analysis shows that E_{2u} mode ($\omega_0=20.5$ meV) couples with CEF excitation between $|\pm 3/2\rangle$ and $|\pm 5/2\rangle$ which has energy $\Delta = 14$ meV. Using the value of g , we can now evaluate the splitting of two axial phonons using Eq. (C13) and with $\mu_{gs}^{el} = 2\mu_B$ which is the magnetic moment for $J = 5/2, m_j = \pm 5/2$

which comes out to be

$$\omega_{ph}^+ - \omega_{ph}^- \approx 0.3 \tanh\left(\frac{2\mu_B B}{k_B T}\right) \text{ meV} \quad (\text{D21})$$

which indicates a saturation splitting close to 0.3 meV as shown in Fig. 4(c).

-
- [1] H. Zhu, J. Yi, M.-Y. Li, J. Xiao, L. Zhang, C.-W. Yang, R. A. Kaindl, L.-J. Li, Y. Wang, and X. Zhang, Observation of chiral phonons, *Science* **582**, 579 (2018).
- [2] S. R. Tauchert, M. Volkov, D. Ehberger, D. Kazenwadel, M. Evers, H. Lange, A. Donges, A. Book, W. Kreuzpaintner, U. Nowak, and P. Baum, Polarized phonons carry angular momentum in ultrafast demagnetization, *Nature* **602**, 73 (2022).
- [3] C. S. Davies, F. G. N. Fennema, A. Tsukamoto, I. Razdolski, A. V. Kimel, and A. Kirilyuk, Phononic switching of magnetization by the ultrafast Barnett effect, *Nature* **628**, 540–544 (2024).
- [4] H. Ueda, M. García-Fernández, S. Agrestini, C. P. Romao, J. van den Brink, N. A. Spaldin, K.-J. Zhou, and U. Staub, Chiral phonons in quartz probed by X-rays, *Nature* **618**, 946 (2023).
- [5] K. Ishito, H. Mao, Y. Kousaka, Y. Togawa, S. Iwasaki, T. Zhang, S. Murakami, J.-i. Kishine, and T. Satoh, Truly chiral phonons in α -HgS, *Nature Physics* **19**, 35 (2023).
- [6] H. Ueda, A. Nag, C. P. Romao, M. García-Fernández, K.-J. Zhou, and U. Staub, Chiral phonons in polar LiNbO₃, *Nat. Comm.* **17**, 212 (2025).
- [7] D. M. Juraschek, R. M. Geilhufe, H. Zhu, M. Basini, P. Baum, A. Baydin, S. Chaudhary, M. Fechner, B. Flebus, G. Grissonnanche, A. I. Kirilyuk, M. Lemesko, S. F. Maehrlein, M. Mignolet, S. Murakami, Q. Niu, U. Nowak, C. P. Romao, H. Rostami, T. Satoh, N. A. Spaldin, H. Ueda, and L. Zhang, Chiral phonons, *Nature Physics* **21**, 1532 (2025).
- [8] D. M. Juraschek and N. A. Spaldin, Orbital magnetic moments of phonons, *Phys. Rev. Mater.* **3**, 064405 (2019).
- [9] Y. Ren, C. Xiao, D. Saparov, and Q. Niu, Phonon Magnetic Moment from Electronic Topological Magnetization, *Phys. Rev. Lett.* **127**, 186403 (2021).
- [10] X.-W. Zhang, Y. Ren, C. Wang, T. Cao, and D. Xiao, Gate-tunable phonon magnetic moment in bilayer graphene, *Phys. Rev. Lett.* **130**, 226302 (2023).
- [11] S. Chaudhary, D. M. Juraschek, M. Rodriguez-Vega, and G. A. Fiete, Giant effective magnetic moments of chiral phonons from orbit-lattice coupling, *Phys. Rev. B* **110**, 094401 (2024).
- [12] L. Zhang and Q. Niu, Chiral phonons at high-symmetry points in monolayer hexagonal lattices, *Phys. Rev. Lett.* **115**, 115502 (2015).
- [13] S. Streib, Difference between angular momentum and pseudoangular momentum, *Phys. Rev. B* **103**, L100409 (2021).
- [14] L. Allen, M. W. Beijersbergen, R. J. C. Spreeuw, and J. P. Woerdman, Orbital angular momentum of light and the transformation of Laguerre-Gaussian laser modes, *Phys. Rev. A* **45**, 8185 (1992).
- [15] L. Gao, S. Prokhorenko, Y. Nahas, and L. Bellaiche, Dynamical Multiferroicity and Magnetic Topological Structures Induced by the Orbital Angular Momentum of Light in a Nonmagnetic Material, *Phys. Rev. Lett.* **131**, 196801 (2023).
- [16] D. A. Garanin and E. M. Chudnovsky, Angular momentum in spin-phonon processes, *Phys. Rev. B* **92**, 024421 (2015).
- [17] J. J. Nakane and H. Kohno, Angular momentum of phonons and its application to single-spin relaxation, *Phys. Rev. B* **97**, 174403 (2018).
- [18] C. Jia, D. Ma, A. F. Schäffer, and J. Berakdar, Twisted magnon beams carrying orbital angular momentum, *Nature Communications* **10**, 2077 (2019).
- [19] T. Wang, H. Sun, X. Li, and L. Zhang, Chiral phonons: Prediction, verification, and application, *Nano Letters* **24**, 4311 (2024).
- [20] H. Chen, W. Zhang, Q. Niu, and L. Zhang, Chiral phonons in two-dimensional materials, *2D Mater.* **6**, 012002 (2019).
- [21] H. Chen, W. Wu, S. A. Yang, X. Li, and L. Zhang, Chiral phonons in kagome lattices, *Phys. Rev. B* **100**, 094303 (2019).
- [22] D. Yao and S. Murakami, Conversion of chiral phonons into magnons in ferromagnets and antiferromagnets, *J. Phys. Soc. Japan* **93**, 034708 (2024).
- [23] A. Ptok, A. Kobińska, M. Sternik, J. Łażewski, P. T. Jochym, A. M. Oleś, S. Stankov, and P. Piekarczyk, Chiral phonons in the honeycomb sublattice of layered CoSn-like compounds, *Phys. Rev. B* **104**, 054305 (2021).
- [24] L. Zhang and Q. Niu, Angular Momentum of Phonons and the Einstein–de Haas Effect, *Phys. Rev. Lett.* **112**, 085503 (2014).
- [25] R. M. Geilhufe, V. Juričić, S. Bonetti, J.-X. Zhu, and A. V. Balatsky, Dynamically induced magnetism in KTaO₃, *Phys. Rev. Research* **3**, L022011 (2021).
- [26] A. Zabalo, C. E. Dreyer, and M. Stengel, Rotational g factors and Lorentz forces of molecules and solids from density functional perturbation theory, *Phys. Rev. B* **105**, 094305 (2022).
- [27] D. M. Juraschek, M. Fechner, A. V. Balatsky, and N. A. Spaldin, Dynamical multiferroicity, *Phys. Rev. Mater.* **1**, 014401 (2017).
- [28] R. Merlin, Magnetophononics and the chiral phonon misnomer, *PNAS nexus* **4**, pgaf002 (2025).
- [29] C. P. Romao, R. Catena, N. A. Spaldin, and M. Matas, Chiral phonons as dark matter detectors, *Phys. Rev. Res.* **5**, 043262 (2023).

- [30] R. Merlin, Unraveling the effect of circularly polarized light on reciprocal media: Breaking time reversal symmetry with non-Maxwellian magnetic-esque fields, *Phys. Rev. B* **110**, 094312 (2024).
- [31] H. Mustafa, C. Nnokwe, G. Ye, M. Fang, S. Chaudhary, J.-A. Yan, K. Wu, C. J. Cunningham, C. M. Hemesath, A. J. Stollenwerk, P. M. Shand, E.-H. Yang, G. A. Fiete, R. He, and W. Jin, Origin of large effective phonon magnetic moments in monolayer MoS₂, *ACS nano* **19**, 11241 (2025).
- [32] X.-W. Zhang, Y. Ren, C. Wang, T. Cao, and D. Xiao, Gate-tunable phonon magnetic moment in bilayer graphene, *Phys. Rev. Lett.* **130**, 226302 (2023).
- [33] F. G. Hernandez, A. Baydin, S. Chaudhary, F. Tay, I. Katayama, J. Takeda, H. Nojiri, A. K. Okazaki, P. H. Rapp, E. Abramof, *et al.*, Observation of interplay between phonon chirality and electronic band topology, *Science advances* **9**, eadj4074 (2023).
- [34] R. M. Geilhufe and W. Hergert, Electron magnetic moment of transient chiral phonons in KTaO₃, *Phys. Rev. B* **107**, L020406 (2023).
- [35] R. M. Geilhufe, Dynamic electron-phonon and spin-phonon interactions due to inertia, *Phys. Rev. Research* **4**, L012004 (2022).
- [36] D. Lujan, J. Choe, S. Chaudhary, G. Ye, C. Nnokwe, M. Rodriguez-Vega, J. He, F. Y. Gao, T. N. Nunley, E. Baldini, *et al.*, Spin-orbit exciton-induced phonon chirality in a quantum magnet, *Proceedings of the National Academy of Sciences* **121**, e2304360121 (2024).
- [37] N. Shabala and R. M. Geilhufe, Phonon inverse Faraday effect from electron-phonon coupling, *Phys. Rev. Lett.* **133**, 266702 (2024).
- [38] J. Luo, T. Lin, J. Zhang, X. Chen, E. R. Blackert, R. Xu, B. I. Yakobson, and H. Zhu, Large effective magnetic fields from chiral phonons in rare-earth halides, *Science* **382**, 698 (2023).
- [39] T. F. Nova, A. Cartella, A. Cantaluppi, M. Först, D. Bossini, R. V. Mikhaylovskiy, A. V. Kimel, R. Merlin, and A. Cavalleri, An effective magnetic field from optically driven phonons, *Nat. Phys.* **13**, 132 (2017).
- [40] D. M. Juraschek, T. Neuman, and P. Narang, Giant effective magnetic fields from optically driven chiral phonons in 4f paramagnets, *Phys. Rev. Research* **4**, 013129 (2022).
- [41] M. Basini, M. Pancaldi, B. Wehinger, M. Udina, V. Unikandanunni, T. Tadano, M. Hoffmann, A. Balatsky, and S. Bonetti, Terahertz electric-field-driven dynamical multiferroicity in SrTiO₃, *Nature* **628**, 534 (2024).
- [42] X. Chen, X. Lu, S. Dubey, Q. Yao, S. Liu, X. Wang, Q. Xiong, L. Zhang, and A. Srivastava, Entanglement of single-photons and chiral phonons in atomically thin WSe₂, *Nat. Phys.* **15**, 221 (2019).
- [43] S. Zhang, Z. Huang, M. Du, T. Ying, L. Du, and T. Zhang, The chirality of phonons: Definitions, symmetry constraints, and experimental observation, *arXiv:2503.22794* (2025).
- [44] X. Gonze, B. Amadon, G. Antonius, F. Arnardi, L. Baguet, J.-M. Beuken, J. Bieder, F. Bottin, J. Bouchet, E. Bousquet, N. Brouwer, F. Bruneval, G. Brunin, T. Cavignac, J.-B. Charraud, W. Chen, M. Côté, S. Cottenier, J. Denier, G. Geneste, P. Ghosez, M. Giantomassi, Y. Gillet, O. Gingras, D. R. Hamann, G. Hautier, X. He, N. Helbig, N. Holzwarth, Y. Jia, F. Jollet, W. Lafargue-Dit-Hauret, K. Lejaeghere, M. A. L. Marques, A. Martin, C. Martins, H. P. C. Miranda, F. Naccarato, K. Persson, G. Petretto, V. Planes, Y. Pouillon, S. Prokhorenko, F. Ricci, G.-M. Rignanese, A. H. Romero, M. M. Schmitt, M. Torrent, M. J. van Setten, B. Van Troeye, M. J. Verstraete, G. Zerah, and J. W. Zwanziger, The ABINIT project: Impact, environment and recent developments, *Comput. Phys. Commun.* **248**, 107042 (2020).
- [45] J. P. Perdew, K. Burke, and M. Ernzerhof, Generalized gradient approximation made simple, *Phys. Rev. Lett.* **77**, 3865 (1996).
- [46] S. Grimme, J. Antony, S. Ehrlich, and H. Krieg, A consistent and accurate *ab initio* parametrization of density functional dispersion correction (DFT-D) for the 94 elements H–Pu, *J. Chem. Phys.* **132**, 154104 (2010).
- [47] S. Chaudhary, C. P. Romao, and D. M. Juraschek, *Anomalous phonon magnetic moments – supplementary data* (2025).
- [48] M. Che, J. Liang, Y. Cui, H. Li, B. Lu, W. Sang, X. Li, X. Dong, S. Zhang, T. Sun, *et al.*, Magnetic order induced truly chiral phonons in a ferromagnetic Weyl semimetal, *arXiv:2411.03754* (2024).
- [49] R. Yang, Y.-Y. Zhu, M. Steigleder, X.-G. Qiu, T.-T. Zhang, and M. Dressel, Inherent circular dichroism of phonons in magnetic weyl semimetal co3sn2s2, *arXiv:2410.21775* (2024).
- [50] G. Schaack, Observation of circularly polarized phonon states in an external magnetic field, *J. Phys. C: Solid State Phys.* **9**, 297 (1976).
- [51] G. Schaack, Magnetic Field Dependent Splitting of Doubly Degenerate Phonon States in Anhydrous Cerium-Trichloride, *Z. Physik B* **26**, 49 (1977).
- [52] E. Kroumova, M. I. Aroyo, J. M. Perez-Mato, A. Kirov, C. Capillas, S. Ivantchev, and H. Wondratschek, Bilbao Crystallographic Server: useful databases and tools for phase-transition studies, *Phase Transitions* **76**, 155 (2003).
- [53] H. Rostami and E. Cappelluti, Strain-driven chiral phonons in two-dimensional hexagonal materials, *Phys. Rev. B* **105**, 195431 (2022).
- [54] X. Li, J. Zhong, J. Cheng, H. Chen, H. Wang, J. Liu, D. Sun, L. Zhang, and J. Zhou, Chiral phonon activated spin Seebeck effect in chiral materials, *Sci. China Phys., Mech. Astron* **67**, 237511 (2024).
- [55] M. Gao, W. Zhang, and L. Zhang, Nondegenerate chiral phonons in graphene/hexagonal boron nitride heterostructure from first-principles calculations, *Nano Lett.* **18**, 4424 (2018).
- [56] A. Jain, S. P. Ong, G. Hautier, W. Chen, W. D. Richards, S. Dacek, S. Cholia, D. Gunter, D. Skinner, G. Ceder, *et al.*, Commentary: The Materials Project: A materials genome approach to accelerating materials innovation, *APL Materials* **1** (2013).
- [57] K. Persson, *Materials data on GaAs (SG:216) by Materials Project* (2014).
- [58] D. M. Juraschek and P. Narang, Shaken not strained, *Nat. Phys.* **16**, 900 (2020).
- [59] Y.-P. Lin and R. M. Nandkishore, Complex charge density waves at van hove singularity on hexagonal lattices: Haldane-model phase diagram and potential realization in the kagome metals aV_3sb_5 ($a=k, rb, cs$), *Phys. Rev. B* **104**, 045122 (2021).
- [60] B. Zenker, H. Fehske, H. Beck, C. Monney, and A. R.

- Bishop, Chiral charge order in $1t\text{-tise}_2$: Importance of lattice degrees of freedom, *Phys. Rev. B* **88**, 075138 (2013).
- [61] S. Zhang, K. Luo, and T. Zhang, Understanding chiral charge-density wave by frozen chiral phonon, *npj Computational Materials* **10**, 264 (2024).
- [62] S.-L. Yu and J.-X. Li, Chiral superconducting phase and chiral spin-density-wave phase in a hubbard model on the kagome lattice, *Phys. Rev. B* **85**, 144402 (2012).
- [63] R. Sutcliffe, K. Hart, S. Chaudhary, and A. Paramakanti, Pseudo-chiral phonon splitting from octupolar magnetic order, [arXiv:2506.18978](https://arxiv.org/abs/2506.18978) (2025).
- [64] R. Xue, Z. Qiao, Y. Gao, and Q. Niu, Anisotropic gyromagnetic ratio and orthogonal einstein-de haas effect, [arXiv:2601.17474](https://arxiv.org/abs/2601.17474) (2026).
- [65] K. Kim, E. Vetter, L. Yan, C. Yang, Z. Wang, R. Sun, Y. Yang, A. H. Comstock, X. Li, J. Zhou, *et al.*, Chiral-phonon-activated spin Seebeck effect, *Nat. Mater.* **22**, 322 (2023).
- [66] K. Ohe, H. Shishido, M. Kato, S. Utsumi, H. Matsuura, and Y. Togawa, Chirality-induced selectivity of phonon angular momenta in chiral quartz crystals, *Phys. Rev. Lett.* **132**, 056302 (2024).
- [67] L. Zhang and Q. Niu, Chiral Phonons at High-Symmetry Points in Monolayer Hexagonal Lattices, *Phys. Rev. Lett.* **115**, 115502 (2015).
- [68] G. Grissonnanche, A. Legros, S. Badoux, E. Lefrançois, V. Zlatko, M. Lizaire, F. Laliberté, A. Gourgout, J. S. Zhou, S. Pyon, T. Takayama, H. Takagi, S. Ono, N. Doiron-Leyraud, and L. Taillefer, Giant thermal Hall conductivity in the pseudogap phase of cuprate superconductors, *Nature* **571**, 376 (2019).
- [69] G. Grissonnanche, S. Thériault, A. Gourgout, M. E. Boulanger, E. Lefrançois, A. Ataei, F. Laliberté, M. Dion, J. S. Zhou, S. Pyon, T. Takayama, H. Takagi, N. Doiron-Leyraud, and L. Taillefer, Chiral phonons in the pseudogap phase of cuprates, *Nat. Phys.* **16**, 1108 (2020).
- [70] S. Park and B.-J. Yang, Phonon angular momentum Hall effect, *Nano Lett.* **20**, 7694 (2020).
- [71] G. Aeppli, A. V. Balatsky, H. M. Rønnow, and N. A. Spaldin, Hidden, entangled and resonating order, *Nat. Rev. Mater.* **5**, 477 (2020).
- [72] A. Shitade, H. Watanabe, and Y. Yanase, Theory of orbital magnetic quadrupole moment and magnetoelectric susceptibility, *Phys. Rev. B* **98**, 020407 (2018).
- [73] X. H. Verbeek, A. Urru, and N. A. Spaldin, Hidden orders and (anti-) magnetoelectric effects in Cr_2O_3 and $\alpha\text{-Fe}_2\text{O}_3$, *Physical Rev. Res.* **5**, L042018 (2023).
- [74] A. Urru, J.-R. Soh, N. Qureshi, A. Stunault, B. Roessli, H. M. Rønnow, and N. A. Spaldin, Neutron scattering from local magnetoelectric multipoles: A combined theoretical, computational, and experimental perspective, *Phys. Rev. Res.* **5**, 033147 (2023).
- [75] J.-R. Soh, M. E. Merkel, L. V. Pourovskii, I. Živković, O. Malanyuk, J. Pásztorová, S. Francoual, D. Hirai, A. Urru, D. Tolj, *et al.*, Spectroscopic signatures and origin of hidden order in $\text{Ba}_2\text{MgReO}_6$, *Nat. Comm.* **15**, 10383 (2024).
- [76] E. Kroumova, M. Aroyo, J. Perez-Mato, A. Kirov, C. Capillas, S. Ivantchev, and H. Wondratschek, Bilbao crystallographic server: useful databases and tools for phase-transition studies, *Phase Transitions: A Multinational Journal* **76**, 155 (2003).